Graphical Methods for Reaction Distribution in a Reactive Distillation Column

Jae W. Lee, Steinar Hauan, and Arthur W. Westerberg
Dept. of Chemical Engineering and Institute for Complex Engineered Systems, Carnegie Mellon University, Pittsburgh, PA 15213

Visual methods of determining how to distribute reaction zones within a binary reactive distillation column were studied using both the Ponchon–Savarit and McCabe–Thiele methods modified to account for the reaction. Two types of reactions are compatible with a totally binary system: isomerization and dimerization. For isomerization with a heavy reactant and a light product, both diagrams indicate the potential for a pinch point if the reaction zone is in the stripping section and no such potential if the zone is in the rectifying section. These same diagrams show that the column will have fewer stages and less usage of utility to yield the same final top and bottom products with the reaction in the rectifying section. The situation reverses if the reactant is the light species for isomerization, suggesting reaction should then take place in the stripping section. The heat effect from the isomerization reaction is considered for four cases depending on whether the reaction is endothermic or exothermic. Even if the heat of the isomerization is dominant, the results do not change: with a heavy reactant and a light product, the separation performance is better when the reaction takes place in the rectifying section. In the dimerization reaction, where two light reactants form a heavy product, the light reactant enriches as we go down the column and the composition profile is reversed in a Ponchon–Savarit diagram with the reaction in the rectifying section even if there is no pinch point. Results on the location of reaction zones are confirmed by rigorous simulations.

Introduction

Reactive distillation is an attractive unit process due to its integrated functionality of reaction and separation compared to a conventional unit process that has single functionality. This integrated functionality can provide us with dramatic economic effects in terms of initial investment and operating costs such as the methyl acetate production system (Agreda and Partin, 1984; Agreda et al., 1990; Siirola, 1995). The most serious restriction in employing reactive distillation is that reaction temperature should coincide with the distillation range (DeGarmo et al., 1992). That means we should develop new catalysts available for the proper temperature range in reactive distillation columns, if needed. Despite this weakness, reactive distillation can lead to complete conversion for systems with equilibrium-limited reactions since products are removed continuously as they are being formed. Also, the heat of reaction can be naturally integrated with the distillation process. These advantages of adopting reactive distillation technology have prompted many studies on designing a reactive distillation column.

Doherty's group at the University of Massachusetts (Barbosa and Doherty, 1987a,b; Doherty, 1990) developed an elegant method to represent reactive residue diagrams and proposed a reactive azeotrope as a fixed boundary of reactive distillation under the assumption of chemical equilibrium. Based on these studies, Barbosa and Doherty (1998a,b) developed a technique for designing single-feed and double-feed reactive distillation columns with the assumptions of constant molal overflow (CMO) and reaction equilibrium in the transformed coordinates. Espinosa et al. (1993) proposed Ponchon–Savarit diagrams in the transformed composition-

Correspondence concerning this article should be addressed to A. W. Westerberg.

enthalpy space to simultaneously account for heat and mass balances under the assumption of reaction equilibrium. Buzad and Doherty (1994, 1995) continued their studies with kinetically controlled reactions in terms of the Damköhler number (Da) instead of the relaxation of reaction equilibrium. But their studies were still carried out under the assumption of CMO with isomolar reaction and equal liquid holdup on each tray. Recently, Okasinski and Doherty (1998) developed a design method applicable to the reactive distillation system, which considers the heat effects, nonideal vapor/liquid equilibrium, and the variable residence time.

Serafimov's group in Russia (Balashov and Serafimov, 1980; Pisarenko and Serafimov, 1988) has developed a method of static analysis, a theoretical framework for analyzing reactive rectification columns. Pisarenko et al. (1995, 1997) developed a procedure for evaluating the feasibility of a reactive distillation column in terms of the limiting steady state at maximum reaction conversion. Giessler et al. (1998) applied this static analysis procedure to generate feasible design alternatives.

In the transformed coordinates, one is likely to lose some physical insights. The overall and stagewise reaction conversions are not easily accessible since they project the original composition space into a reduced space by the stoichiometric line regardless of the extent of reaction as shown by Bessling et al. (1997) and Stichlmair and Fair (1998). Thus, we may not have an intuitive feel for what is really happening inside a column. The static analysis approach accounts only for the overall reaction conversion in a column and does not address the extent of reaction on each stage. Hence, it cannot show pinch situations such as reactive azeotropes (Barbosa and Doherty, 1987a) and reactive fixed points (Hauan et al., 1999) arising from the colinearity of reacting, separating, and mixing as individual phenomena.

In an attempt to extend the visual insights available for reactive distillation columns, we recently presented reactive Ponchon–Savarit and McCabe–Thiele diagrams (Lee et al., 2000b,c) derived from five previous analytical results: (1) the reaction difference point characterizing the generated flow by reaction (Hauan et al., 1996, 1999); (2) the decomposition of the total stoichiometric coefficient vector into reactant and product coefficient vectors to obviate an infinite composition space (Lee et al., 2000a); (3) the generalized cascade difference point from the linear combination of the reaction difference point, the feed and product compositions (Hauan 1998, Hauan et al., 2000), which moves as we step up or off the the stages due to reaction; (4) the pseudofeed composition from combining product compositions (Lee et al., 2000a), from which the extent of reaction is geometrically available by a reactive lever rule; and (5) the linear composition changes caused by reaction in the original composition space (Hauan et al., 1999).

In this work, we illustrate how to distribute reaction zones within a column using the McCabe–Thiele and Ponchon–Savarit methods for a given reaction conversion by adjusting the catalyst holdup on each stage. We first show McCabe–Thiele diagrams for a binary isomerization with different arrangements of reaction zones in a column and present the configuration causing a pinch point. Then, we consider the heat effect from reaction in McCabe–Thiele and Ponchon–Savarit diagrams for four different cases with exothermic and endothermic isomerization reactions. Second, we draw Ponchon–Savarit diagrams for a dimerization reaction with different locations of reaction zones. We confirm the graphical results by computer simulation with the isomerization of 1,4-dichloro-2-butene converting into 1,2-dichloro-3-butene under reaction equilibrium. We also present simulation results for the isomerization of cyclohexanone oxime to epsilon-caprolactam and the dimerization reaction of isobutyraldehyde to isobutylisobutyrate.

Reaction Distribution by McCabe–Thiele Diagrams for Isomerization in a Column

We should maintain the constant molal overflow (CMO) assumption to develop the McCabe–Thiele method for reactive distillation. Thus, we take the following isomerization reaction in which there is no change in the total number of moles, since one mol of *heavy* reactant $R1$ converts into one mol of *light* product $P1$.

$$R1 \Leftrightarrow P1. \tag{1}$$

The heat of reaction is generally negligible compared to the enthalpy of vaporization and two isomers have almost the same heat of vaporization. We provide most of component $R1$ with a small amount of component $P1$ in the feed stream. We further assume that the compositions on all reactive stages are within the forward reaction region. We consider three different column configurations with this isomerization reaction occurring on the feed stage or in either end section.

Reactive operating lines of the reaction zone in the rectifying section

The overall and component balance equations around the reactive rectifying section in Figure 1 are

$$V_{n+1} = L_n + D - \nu_T \xi_n \tag{2}$$

$$V_{n+1} y_{n+1} = L_n x_n + D x_D - \boldsymbol{\nu} \xi_n. \tag{3}$$

Here, ξ_n is the accumulated sum of reaction molar turnover flow rate until the nth stage from the top; ν_T is the total sum of the stoichiometric coefficients, which is zero for reaction (1); and $\boldsymbol{\nu}$ is stoichiometric coefficient vector and $[-1, 1]^T$ for this reaction. Thus, the reaction difference point is infinite, that is, $\delta_R = \boldsymbol{\nu}/\nu_T = [-1, 1]^T/0$. We decompose the stoichiometric coefficient vector into the product coefficient vector $c_P = [0, 1]^T$ and the reactant coefficient vector $c_R = [1, 0]^T$ to construct a McCabe–Thiele diagram within a finite composition space. Based on this decomposition of the stoichiometric coefficient vector, we can rearrange Eq. 3 into Eq. 4 with the constant vapor and liquid flow rates in the rectifying section for product $P1$. There are several operating lines parallel to each other for the same slope (L/V) in Eq. 4, since the y-intercept is changing stage-to-stage in terms of the accumulated sum of reaction molar turnover flowrate, ξ_n, which will increase as we go down the column.

If we step off the stage from the top, the first operating line in the rectifying section meets the 45-degree line at the distillate composition, x_D, in Figure 2. The second operating line crosses the $y = x$ line to the left of the distillate compo-

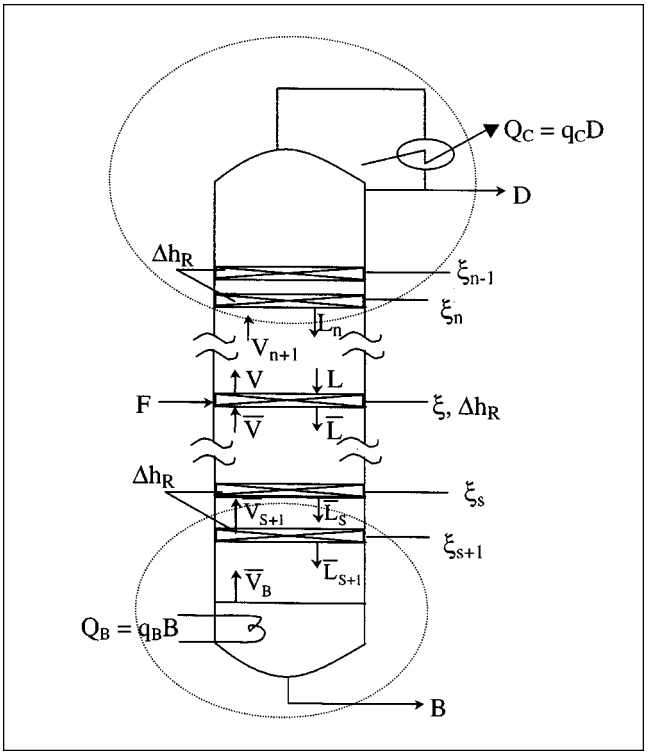

Figure 1. A reactive distillation column with separate reaction zones.

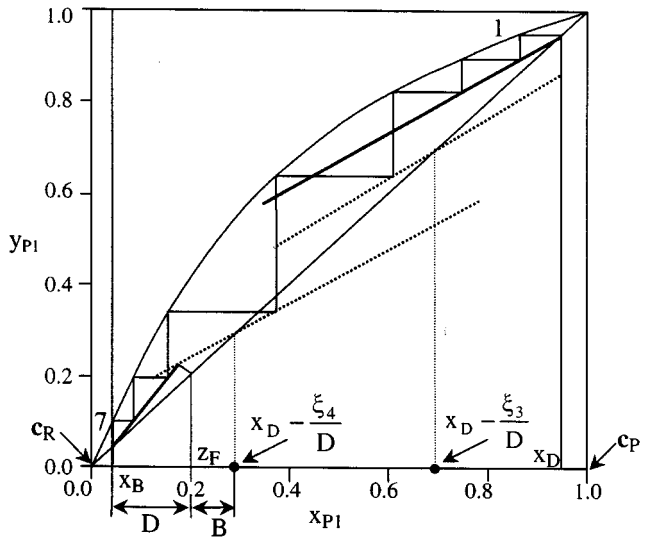

Figure 2. The McCabe–Thiele method for reactive distillation with the isomerization reaction of a heavy reactant producing a light product occurs in the rectifying section.

●: Difference point (hereafter); ···· : reactive operating line (hereafter in McCabe–Thiele diagrams); —— : nonreactive operating line (hereafter in McCabe–Thiele diagrams).

sition for a given reaction molar turnover flow rate. We will refer to these moving intersection points as *difference points*, and we can easily determine these difference points from the reactive operating lines and the 45-degree line by using Eq. 4 and allowing equal vapor and liquid compositions. The difference points in Eq. 5 will move to the left as we go down the column in Figure 2:

$$y_{n+1} = \frac{L}{V} x_n + \left(1 - \frac{L}{V}\right) x_D - \frac{\xi_n}{V} \tag{4}$$

$$x_n = x_D - \frac{\xi_n}{D}. \tag{5}$$

The operating line of the stripping section and the *q*-line of the feed stage are the same as in nonreactive distillation because we have no reaction in the stripping section and at the feed stage. In Figure 2, we take the feed stream with the mixed phase. The slope of the *q*-line is negative.

In terms of Eqs. 4 and 5, the operating lines in the rectifying section move down and the distance between the equilibrium curve and the operating line increases as we move down the column. Consequently, the composition change for each equilibrium stage becomes larger, thus improving the separation efficiency.

Reactive operating line of the reaction zone in the stripping section

When the isomerization reaction takes place in the stripping section, the material balances around the lower envelope in Figure 1 become as follows:

$$\bar{V}_{s+1} = \bar{L}_s - B + \nu_T \xi_{s+1} \tag{6}$$

$$\bar{V}_{s+1} y_{s+1} = \bar{L}_s x_s - B x_B + \boldsymbol{\nu} \xi_{s+1}. \tag{7}$$

If we set the vapor and liquid flow rates to be constant, substitute Eq. 6 into Eq. 7, and then decompose the stoichiometric coefficient vector as previously shown, we get the operating line for the stripping section in Eq. 8. This equation is scalar and represents the change in the mol fraction of component $P1$. Equation 9 describes how the difference points move along the line $y = x$. The first nonreactive operating line will meet the 45-degree line at the bottom product composition in Figure 3. The second reactive operating line will intersect the left extension of the 45-degree line for a given reaction molar turnover flow rate:

$$y_{s+1} = \frac{\bar{L}}{\bar{V}} x_s - \left(\frac{\bar{L}}{\bar{V}} - 1\right) x_B + \frac{\xi_{s+1}}{\bar{V}} \tag{8}$$

$$x_s = x_B - \frac{\xi_{s+1}}{B}. \tag{9}$$

Since the total sum of stoichiometric coefficients, ν_T, is zero in Eq. 6, the slope of the operating line, $\bar{L}/\bar{V}$, is greater than one and the operating lines are steeper than 45 degrees.

We obtain an important insight from Eqs. 8 and 9, which shows that the operating line will move up as we step up the stages due to the last term on the right side of Eq. 8, in Figure 3. The accumulated sum of the reaction molar turnover flow rate, ξ_{s+1}, from the bottom stage to stage $(s+1)$ will

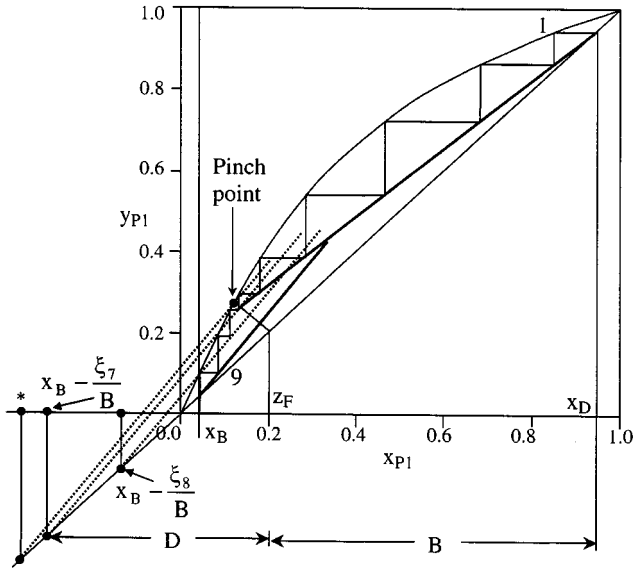

Figure 3. The McCabe–Thiele method for reactive distillation with the isomerization reaction of a heavy reactant producing a light product occurs in the stripping section.

*: The difference point causing a pinch point.

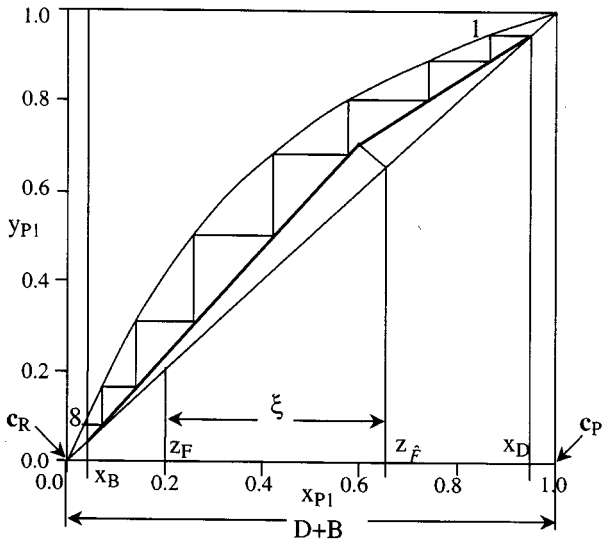

Figure 4. The McCabe–Thiele method for reactive distillation with the isomerization reaction of a heavy reactant producing a light product occurs on the feed stage.

increase in the forward reaction as we go up the column toward the feed stage. All operating lines in the stripping section are parallel to each other because the slope, $\bar{L}/\bar{V}$, is the same for all lines. For an additional reactive stage with the mark (*) in Figure 3, we can have a pinch point at which the operating line in the stripping section intersects the equilibrium curve.

The reaction zone in the feed section

If the isomerization reaction occurs only on the feed stage as in Figure 4, the operating lines in the rectifying and stripping sections are the same as in a nonreactive distillation column. Since the composition changes are caused by the reaction that takes place only on the feed stage; this is nearly the same configuration as a reactor followed by a nonreactive distillation column, except that there is a phase equilibrium between vapor and liquid streams in the reactive feed section. The intersection point between the operating lines in the rectifying and stripping sections is somewhere a point linearly shifted from the feed composition. In terms of total balance in Eqs. 10 to 11, which are vectorial forms, we can determine the intersection point that lies between the straight line connecting the top and bottom product compositions. We can identify the intersection point as the pseudofeed composition, $z_{\hat{F}}$, which is the linear combination of top and bottom product compositions in Eq. 13. If we substitute Eq. 10 into Eq. 11 and decompose the stoichiometric vector $\boldsymbol{\nu}$ into the product and the reactant coefficient vectors, we obtain Eq. 12. Hence, the pseudofeed composition shifts to the right of the feed composition by the ratio, $\xi/(D+B)$, in Figure 4:

$$F = B + D - \nu_T \xi \tag{10}$$

$$Fz_F = Bx_B + Dx_D - \boldsymbol{\nu}\xi \tag{11}$$

$$(D+B)(z_F - z_{\hat{F}}) = -\xi(c_P - c_R) \tag{12}$$

$$z_{\hat{F}} = \frac{Dx_D + Bx_B}{D+B}. \tag{13}$$

If we assume that the heat of reaction is negligible to maintain the CMO assumption, the q-line equation is the same as in a nonreactive distillation column. The only difference is that two operating lines in the rectifying and stripping sections meet at the pseudofeed composition. If we take the total and componentwise balance equations around the feed stage in Figure 1, we obtain Eqs. 14 and 15:

$$(V - \bar{V}) = F - (\bar{L} - L) + \nu_T \xi \tag{14}$$

$$y(V - \bar{V}) = Fz_F - x(\bar{L} - L) + \boldsymbol{\nu}\xi. \tag{15}$$

Substituting Eq. 10 into Eq. 14 by considering ν_T is zero in Eqs. 10 and 14, we can arrange Eq. 15 for component $P1$ in Eq. 16:

$$y = \left(\frac{q}{q-1}\right)x - \frac{z_{\hat{F}}}{q-1} \tag{16}$$

$$q = \frac{\bar{L} - L}{F}. \tag{17}$$

The q-line meets the 45-degree line at the pseudofeed composition, $z_{\hat{F}}$, in Figure 4. Two operating lines intersect each other on this q-line.

Summary of reaction distribution with CMO assumption

We compare three cases of different reaction zones with the same isomerization in a reactive distillation column for a given feed composition, feed thermal condition, and product specifications in terms of the McCabe–Thiele diagrams. If we

have the reaction zone in the rectifying section, in the stripping section, and on the feed stage, respectively, then different numbers of stages are required: seven stages as in Figure 2, nine stages as in Figure 3, and eight stages as in Figure 4 for the desired separation. The heat duties in the reboiler and condenser are smaller for the reaction zone in the rectifying section of Figure 2 than the other two cases in Figure 3 and Figure 4, considering the slopes of nonreactive operating lines in both the sections. The reaction conversion of the reaction zone in the rectifying section is also greater than that of the reaction zone in the stripping section, as the reactive amount of the distillate compared to the bottom product is larger. This can be seen in Figures 2 and 3 in terms of relative lengths of top and bottom product flow rates. For the same reaction conversion and product specifications, the rectifying reaction zone in Figure 2 is better than the reactive feed section in Figure 4, when considering the utility consumption and the total number of stages required for the separation. Hence, it is better to locate the reaction zone in the rectifying section if we have a heavy reactant and a light product in a binary isomerization.

What would happen if the isomerization reaction occurs with *light* reactant $R1$ and *heavy* product $P1$? The results are exactly symmetric to the case having the reaction with a heavy reactant. Since the reactant is lighter than the product, we can construct a McCabe–Thiele diagram in terms of light component $R1$ and obtain Eq. 18 for the reactive operating lines of the stripping section. The equation for the difference points in the stripping section is given in Eq. 19 by equating liquid and vapor compositions in Eq. 18. *y*-Intercepts of the reactive operating lines will decrease as we go up the column, since the accumulated sum of reaction molar turnover flow rate, ξ_{s+1}, increases. Thus, the distance between the operating line and the phase equilibrium curve increases. If we have the reaction zone in the rectifying section, the operating lines and the difference points can be expressed by Eqs. 20 and 21 for component $R1$. We can arrive at a pinch point for a certain reaction conversion, since the reactive operating lines will move upward as we go down the column. Therefore, the reaction zone should be in the stripping section for the isomerization reaction with a light reactant and a heavy product:

$$y_{s+1} = \frac{\overline{L}}{\overline{V}} x_s + \left(1 - \frac{\overline{L}}{\overline{V}}\right) x_B - \frac{\xi_{s+1}}{\overline{V}} \tag{18}$$

$$x_s = x_B + \frac{\xi_{s+1}}{B} \tag{19}$$

$$y_{n+1} = \frac{L}{V} x_n + \left(1 - \frac{L}{V}\right) x_D + \frac{\xi_n}{V} \tag{20}$$

$$x_n = x_D + \frac{\xi_n}{D}. \tag{21}$$

Table 1. Four Cases in the Isomerization Reaction for Different Reaction Zones

	Reactant	Product	Reaction	Reaction Zone
Case 1	Heavy	Light	Endothermic	Rectifying section
Case 2	Heavy	Light	Exothermic	Rectifying section
Case 3	Heavy	Light	Endothermic	Stripping section
Case 4	Heavy	Light	Exothermic	Stripping section

These results are the motivation for this work on the locations of reaction zones. We will include the heat effect from the reaction in the next section.

Consideration of the Heat of Reaction in McCabe–Thiele and Ponchon–Savarit Diagrams

We categorize four cases for the type of heat of isomerization reaction in which a heavy reactant produces a light product. We can understand that the reaction zone should be in the rectifying section with a heavy reactant even if the heat of reaction is dominant. Symmetric results can also be conserved for the other isomerization of a light reactant producing a heavy product.

Reaction heat effect in McCabe–Thiele diagrams

The slopes and *y*-intercepts of the operating lines and the *q*-line in the McCabe–Thiele method can be affected by the heat of reaction if the heat of reaction is comparable to the enthalpy of vaporization. This means the CMO assumption does not hold for both the rectifying and stripping sections. We should also modify the formula of the *q*-line for a reactive feed stage, as in Lee et al. (2000c). When the heat of reaction is dominant, we can think of the reactive zones as intercoolers or interheaters, depending on whether the reaction is endothermic or exothermic. If we have intercoolers in the rectifying section and interheaters in the stripping section of a nonreactive distillation column, the slopes of the operating lines in both sections will become closer to the 45-degree line in a McCabe–Thiele diagram (Ho and Keller, 1987; Terranova and Westerberg, 1989). The closer to the 45-degree line the operating lines are, the larger the composition changes for a single equilibrium step. Hence, we can apply these ideas to the design of a reactive distillation column. Table 1 shows four cases of the isomerization reaction of a heavy reactant producing a light product according to the heat of reaction.

Case 1. The best configuration with endothermic isomerization in which a heavy reactant converts into a light product is when the reaction zone is in the rectifying section. Since according to Eq. 4 the slope (L/V) will increase and the corresponding *y*-intercept will decrease as we go down the column, the separation efficiency is better than for an athermic reaction, as in Figure 5a. However, we should compensate for the increased amount of heat from the reaction in the rectifying section by adding heat input to the reboiler.

Case 2. This case has the same reaction with an identical reactant and product as in case 1. But the reaction is exothermic. Thus, the slopes (L/V) of operating lines are decreasing and the corresponding *y*-intercept can increase or decrease, since the second term $(1 - L/V)x_D$ in Eq. 4 increases as we step off the stages. However, if the following relationship (Eq. 22) holds, the *y*-intercepts will decrease as we go down the column, which will cause a large gap between the operating line and the equilibrium curve in Figure 5b. The derivation is available in Part A of the Appendix. The *y*-intercept decreases if the difference in the vapor flow rates for two stages, $(V_n - V_{n+1})$ is less than or equal to the difference in reaction molar turnover flow rates, $(\xi_n - \xi_{n-1})$, in Eq. 22:

$$(V_n - V_{n+1}) \leq (\xi_n - \xi_{n-1}). \tag{22}$$

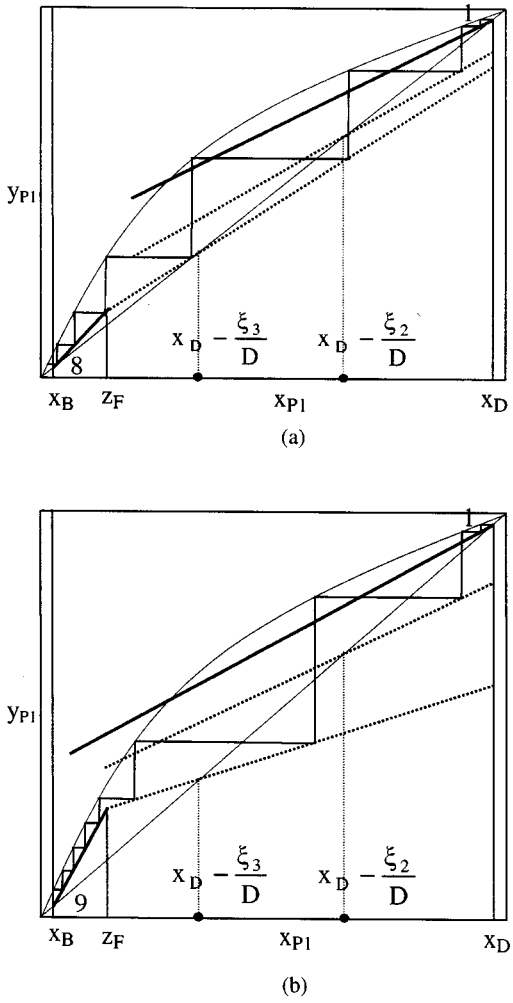

Figure 5. McCabe–Thiele diagrams for reactive distillation considering the heat effect from the isomerization reaction with a heavy reactant and a light product occurring in the rectifying section.

(a) Endothermic reaction; (b) exothermic reaction.

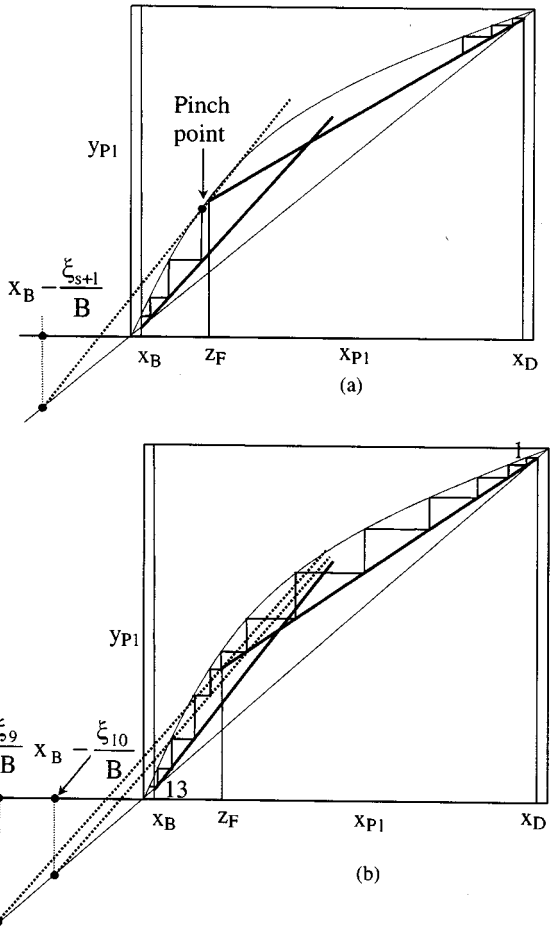

Figure 6. McCabe–Thiele diagrams for reactive distillation considering the heat effect from the isomerization reaction with a heavy reactant and a light product occurring in the stripping section.

(a) Endothermic reaction; (b) exothermic reaction.

Case 3. We deal with the same endothermic reaction as in case 1, but have the reaction zone in the stripping section. This case is the worst, since the operating line in the stripping section will approach the equilibrium curve faster in Figure 6a than in the case of an athermic reaction.

Case 4. If an exothermic reaction with a dominant heat of reaction takes place in the stripping section, we can slow down the speed of the approach of the operating lines toward the equilibrium line. Even in this situation, a pinch point is likely to occur somewhere and we need more stages for the desired separation than in case 1 (8 stages, Figure 5a) and case 2 (9 stages, Figure 5b), as shown in Figure 6b (13 stages).

Ponchon–Savarit diagrams for isomerization in a column

The Ponchon–Savarit method can account for the variation in vapor and liquid flow rates caused by the heat of reaction and different heats of vaporization. This is why the diagram can be constructed with straight lines in a composition-enthalpy space. We assume that the saturated vapor and liquid enthalpies decrease as the amount of more volatile component increases in the mixture. We further assume that the heat of reaction is constant for all compositions. We also present four cases with the same isomerization reaction as in the previous section. The Ponchon–Savarit diagram can be constructed in terms of reactive cascade difference points for reactive stages. The componentwise balance equation around the rectifying and stripping sections are given in Eqs. 3 and 6. By decomposing the stoichiometric coefficient vector, the following material balance equations are available for the reaction zones in the rectifying and stripping sections:

$$V_{n+1}y_{n+1} - L_n x_n = Dx_D - c_P\xi_n + c_R\xi_n = D\delta^r_{R,\,n} \quad (23)$$

$$\overline{V}_{s+1}y_{s+1} - \overline{L}_s x_s = -Bx_B + c_P\xi_n - c_R\xi_n = -B\delta^s_{R,\,s+1}, \quad (24)$$

where $\delta^r_{R,\,n}$ and $\delta^s_{R,\,s+1}$ are reactive cascade difference points for the reactive rectifying and reactive stripping sections in

Eqs. 25 and 28, respectively. Superscripts r and s denote rectifying and stripping sections.

If we denote these reactive cascade difference points in scalar forms for product $P1$ and reactant $R1$ as $\delta^r_{R,\,n,\,P1}$ and $\delta^r_{R,\,n,\,R1}$, we can obtain Eqs. 26 and 27 for a product and a reactant. $\delta^r_{R,\,n,\,P1}$ and $\delta^r_{R,\,n,\,R1}$ are the same as the difference points in Eqs. 5 and 21. In the same sense, $\delta^s_{R,\,s+1,\,P1}$ and $\delta^s_{R,\,s+1,\,R1}$ are scalar reactive cascade difference points for product $P1$ and reactant $R1$ in Eqs. 29 and 30. Note that Eqs. 29 and 30 are the same as Eqs. 9 and 19:

$$\delta^r_{R,\,n} = \frac{Dx_D - c_P\xi_n + c_R\xi_n}{D} \tag{25}$$

$$\delta^r_{R,\,n,\,P1} = x_D - \frac{\xi_n}{D} \tag{26}$$

$$\delta^r_{R,\,n,\,R1} = x_D + \frac{\xi_n}{D} \tag{27}$$

$$\delta^s_{R,s+1} = \frac{Bx_B - c_P\xi_{s+1} + c_R\xi_{s+1}}{B} \tag{28}$$

$$\delta^s_{R,\,s+1,\,P1} = x_B - \frac{\xi_{s+1}}{B} \tag{29}$$

$$\delta^s_{R,\,s+1,\,R1} = x_B + \frac{\xi_{s+1}}{B}. \tag{30}$$

The enthalpy balances around the rectifying and stripping sections in Figure 1 are given in Eqs. 31 and 32:

$$V_{n+1}H_{n+1} - L_nh_n = Dh_D + Q_C + \Delta h_R\xi_n = Dh^r_{R,\,n} \tag{31}$$

$$\overline{V}_{s+1}H_{s+1} - \overline{L}_sh_s = -Bh_B + Q_B - \Delta h_R\xi_{s+1} = -Bh^s_{R,\,s+1}, \tag{32}$$

where

$$h^r_{R,\,n} = h_D + q_C + \Delta h_R\xi_n/D \tag{33}$$

$$h^s_{R,\,s+1} = h_B - q_B + \Delta h_R\xi_{s+1}/B \tag{34}$$

$$q_C = \frac{Q_C}{D} \tag{35}$$

$$q_B = \frac{Q_B}{B}. \tag{36}$$

Here, $h^r_{R,\,n}$ and $h^s_{R,\,s+1}$ are enthalpy difference points for the reactive rectifying and reactive stripping sections; Δh_R is the molar heat of reaction which is negative and positive for exothermic and endothermic reactions; q_C is the molar condenser duty; and q_B is the molar reboiler duty per unit product flow rates.

The remarkable thing is that the slope of the line connecting each cascade reactive difference point is constant in a composition-enthalpy space. The slopes are given in Eqs. 37 and 38 for the rectifying section and Eqs. 39 and 40 for the stripping section. The value of the slope is the molar heat of reaction with negative or positive sign in Eqs. 37 to 40. The detailed derivations are found in Part B of the Appendix:

$$\frac{h^r_{R,\,n+1} - h^r_{R,\,n}}{\delta^r_{R,\,n+1,\,P1} - \delta^r_{R,\,n,\,P1}} = -\Delta h_R \tag{37}$$

$$\frac{h^r_{R,\,n+1} - h^r_{R,\,n}}{\delta^r_{R,\,n+1,\,R1} - \delta^r_{R,\,n,\,R1}} = \Delta h_R \tag{38}$$

$$\frac{h^s_{R,\,s} - h^s_{R,\,s+1}}{\delta^s_{R,\,s,\,P1} - \delta^s_{R,\,s+1,\,P1}} = -\Delta h_R \tag{39}$$

$$\frac{h^s_{R,\,s} - h^s_{R,\,s+1}}{\delta^s_{R,\,s,\,R1} - \delta^s_{R,\,s+1,\,R1}} = \Delta h_R. \tag{40}$$

Case 1 and Case 2. The slope of the straight line connecting cascade reactive difference points for case 1 in Table 1 is negative according to Eq. 37 since the reaction is endothermic. We build Ponchon–Savarit diagrams for case 1 and case 2 in Figures 7a and 7b with the same feed composition, condenser duty, and magnitude of heat of reaction. We have slightly larger heat consumption in reboiling and a smaller total number of trays in case 1 than in case 2. There are trade-offs between the number of trays and utility consumption in the reboiler for case 1 and case 2.

Case 3 and Case 4. If we have the reaction zone in the stripping section, the difference points lie outside the valid composition space in Figures 6 and 8. For the isomerization reaction with a heavy reactant and a light product, the difference points move to the left of the composition space in terms of Eqs. 21 and 27. This clearly has the potential to cause pinch points, since operating lines will be pushed into the equilibrium curve in a McCabe–Thiele diagram and coincide with the equilibrium tie line in the Ponchon–Savarit method. We cannot move up the column from the pinch point at the stage below the feed stage and are unable to move down from the pinch point at the feed stage in Figure 8a. In terms of the operating line in the rectifying section, we also have a pinch point at the feed stage in Figure 8a if we want to perform tray-by-tray calculations from the feed stage to the top stage. In case 3, we encounter these pinch situations from the increased slope of the reactive operating line in the McCabe–Thiele diagram of Figure 6a and the decreased slope of the reactive operating line in the Ponchon–Savarit diagram of Figure 8a. If we have the exothermic reaction in case 4, we can overcome pinch points in Figures 6b and 8b, but we need more stages for the desired separation than in case 2 of Figures 5b and 7b.

Reaction Distribution in the Isomerization of 1,4-Dichloro-2-Butene to 1,2-Dichloro-3-Butene

The isomerization reaction of 1,4-dichloro-2-butene (hereafter DCL2B) to 1,2-dichloro-3-butene (hereafter DCL3B) in Eq. 41 is an essential intermediate step to produce chloroprene (2-chloro-1,3-butadiene), which is a monomer for the production of synthetic rubber. This reaction can occur at the liquid or vapor phases under cuprous chloride and its modified catalysts in the temperature range of 20 to 160°C and the pressure range of 20 to 760 mmHg (Harris and Melchert, 1989; Kadowaki et al., 1975; Gehrmann et al., 1975; Costain and Terry, 1964; Hearne and La France,

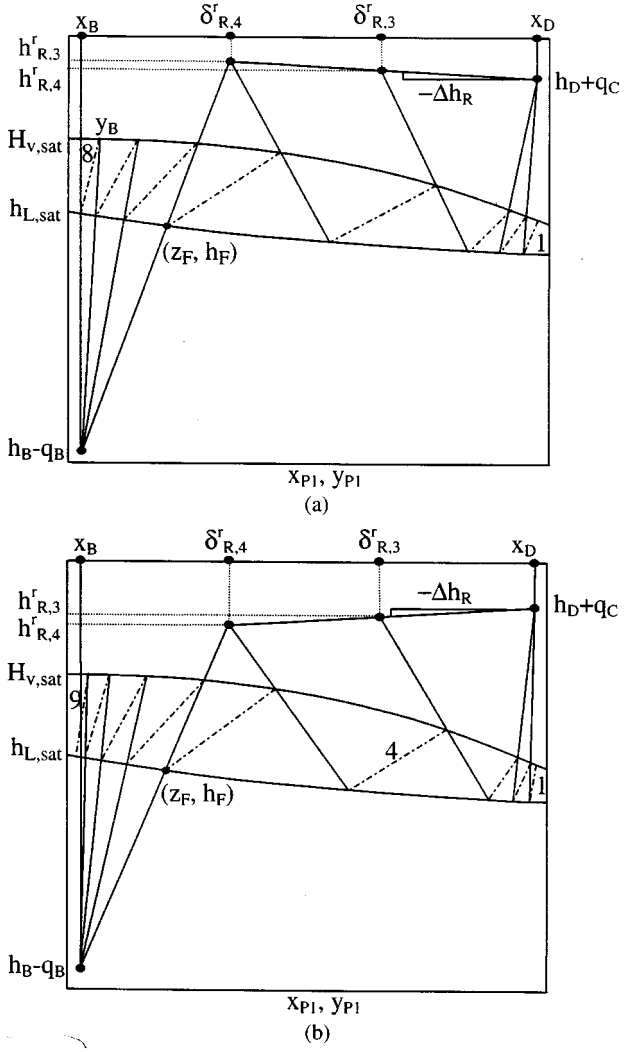

Figure 7. Ponchon–Savarit diagrams for the isomerization with a heavy reactant and a light product in the rectifying section.

(a) Endothermic reaction; (b) exothermic reaction. ·—·—: Equilibrium tie line (hereafter in Ponchon–Savarit diagrams; ——: operating line (hereafter in Ponchon–Savarit diagrams).

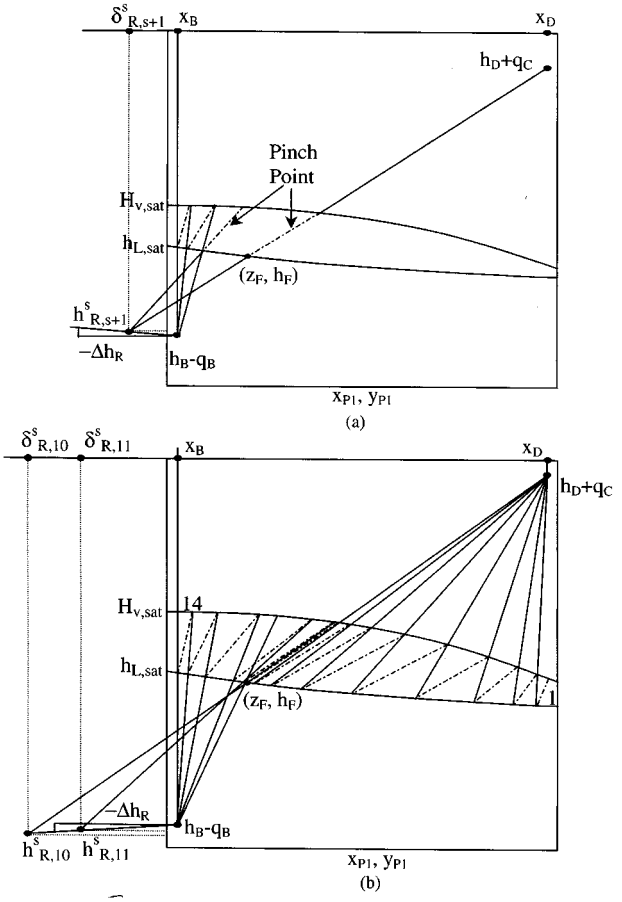

Figure 8. Ponchon–Savarit diagrams for the isomerization with a heavy reactant and a light product in the stripping section.

(a) Endothermic reaction; (b) exothermic reaction.

1948). Since this reaction temperature range overlaps the boiling points of 115 to 156°C found in the reactant and the product, we can apply reactive distillation to this chlorobutene isomerization:

$$ClCH_2CH{=}CHCH_2Cl\ (\text{DCL3B, heavy})$$

$$\Leftrightarrow CH_2{=}CHCHClCH_2Cl\ (\text{DCL3B, light}). \quad (41)$$

The relative volatility of DCL3B is around 2.8 to 3.2 at 1 atm and there is no azeotrope in this mixture according to the Peng–Robinson equation in Aspen Plus. The top product is mostly DCL3B, while most of DCL2B is found in the bottom product. The heat of reaction is negligible (Sittig, 1969) and the McCabe–Thiele method is suitable for determining the location of reactive zones in the column. We understand that we would do well to construct the reaction zone in the rectifying section for the preceding reaction (Eq. 41), as reactant DCL2B is heavier than product DCL3B. We specify product purities for top and bottom products as 0.95 mol fractions. The feed is saturated liquid and consists of DCL2B only.

We construct the McCabe–Thiele diagrams in Figures 9 and 10 without including the feed composition, since the feed composition is outside the product compositions. In the final section we discuss the strange behaviors for the case of the feed composition transcending the bottom composition. An interesting point is that we avoid a possible pinch point at stage 5, in which the reactive operating line meets the equilibrium curve by switching from the reactive operating line to the top operating line in Figure 10. This means that if we have a potential pinch due to a certain reaction conversion, we eliminate the pinch point by changing operating lines or difference points. We perform computer simulation for these cases under the assumption of reaction equilibrium. Our simulation results agree well with results from McCabe–Thiele diagrams in the composition profiles of Table 2. We summarize the simulation results in Table 3. The feed stream is 1000 kmol/h and the compositions are almost the same as in the

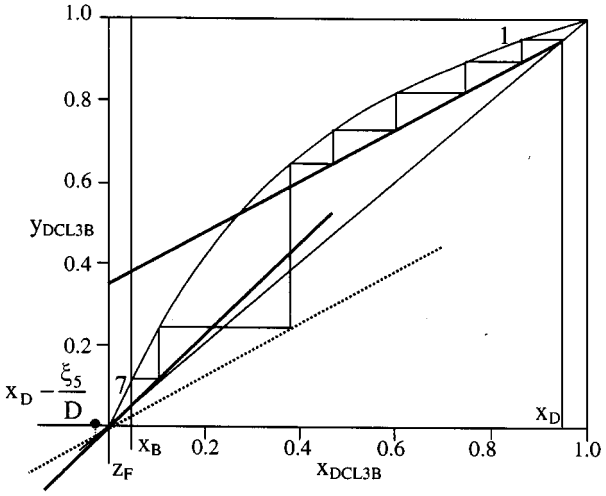

Figure 9. The McCabe–Thiele method for reactive distillation when the isomerization reaction of 1,4-dichloro-2-butene (DCL2B) to 1,2-dichloro-3-butene (DCL3B) occurs in the rectifying section.

McCabe–Thiele diagrams. Considering the total number of stages and the duties in condenser and reboiler in Table 3, the reaction should be in the rectifying section for the isomerization in a reactive distillation column discussed earlier.

Reaction Distribution in the Isomerization of Cyclohexanone Oxime to Epsilon-Caprolactam

Epsilon-caprolactam (ECP) is an important base material used to synthesize nylon and can be produced from the isomerization of cyclohexanone oxime (CYO). This isomerization reaction takes place in the gaseous phase under zeolite catalysts to prevent the problem of the disposal of ammonium sulfate, which is the byproduct in the liquid-phase reaction when sulfuric acid is used as a catalyst (Yashima and Komatsu, 1994; Kajikuri et al., 1994; Kitamura et al., 1990; Bell and Haag, 1990; Sato et al., 1988, 1987; Bell and Chang, 1982). The reaction in Eq. 42 occurs in the temperature range of 150 to 540°C and the pressure range of 1 to 34 atm. The boiling range of ECP and CYO is 283 to 380°C at 5 atm, which is within range of the reaction temperature. The relative volatility of CYO is 2.8 to 3.8 at this pressure from the Peng–Robinson equation of state:

$$C_6H_{10}NOH(\text{CYO, light}) \Leftrightarrow C_5H_{10}CONH(\text{ECP, heavy}). \quad (42)$$

This reaction is exothermic with a heat of reaction -52.2 kJ/mol calculated from the heat of formation for ideal gases (Daubert et al., 1989). The heat of vaporization for the binary mixture varies from 47 kJ/mol to 82 kJ/mol, and is determined by repeated flash calculations. This heat of reaction is comparable to the heat of vaporization. Thus, we first employ the Ponchon–Savarit method, since the vapor and liquid flow rates on each stage will change from this heat effect. The

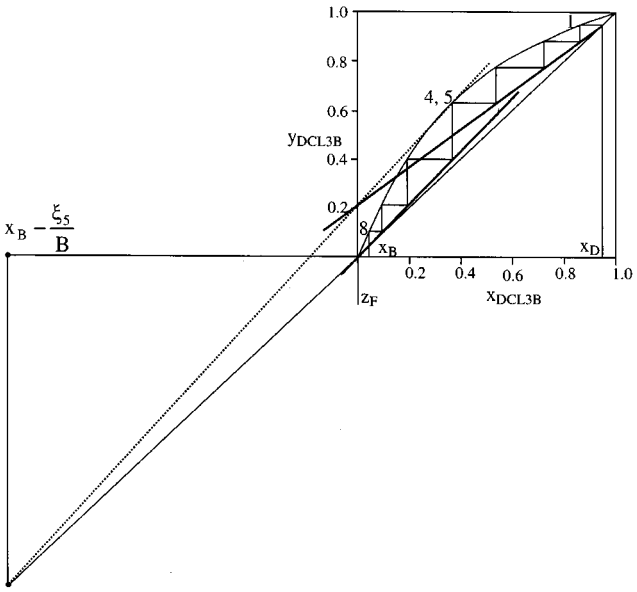

Figure 10. The McCabe–Thiele method for reactive distillation when the isomerization reaction of 1,4-dichloro-2-butene (DCL2B) to 1,2-dichloro-3-butene (DCL3B) occurs in the stripping section.

Table 2. Composition Profiles of DCL3B for Reaction Zones Under Reaction Equilibrium in the Rectifying Section and the Stripping Section

Zone	Rectifying Reaction Zone				Stripping Reaction Zone			
Stage	Liquid		Vapor		Liquid		Vapor	
No.	Fig. 9	Simu.	Fig. 9	Simu.	Fig. 10	Simu.	Fig. 10	Simu.
1	0.86	0.87	0.95	0.95	0.86	0.87	0.95	0.95
2	0.75	0.75	0.89	0.90	0.73	0.73	0.89	0.88
3	0.60	0.61	0.82	0.82	0.55	0.55	0.78	0.76
4	0.48	0.49	0.72	0.72	0.39	0.39	0.63	0.64
5	0.38	0.40	0.64	0.64	0.39	0.40	0.63	0.64
6	0.11	0.11	0.24	0.24	0.20	0.23	0.40	0.45
7	0.05	0.05	0.12	0.12	0.10	0.12	0.21	0.26
8					0.05	0.05	0.10	0.13

Table 3. Comparison of Simulation Results for Both Reaction Zones Under Reaction Equilibrium in the Rectifying and Stripping Sections with the Isomerization in Eq. 41

Reaction Zones	Rectifying Section	Stripping Section
Feed stream		
Flow (kmol/h)	1000	1000
Mol fraction DCL2B	1.0	1.0
Product flow (kmol/h)		
Distillate flow/DCL3B purity	600/95%	600/95%
Bottom flow/DCL2B purity	400/95%	400/95%
Total number of stages	7	8
Feed stage	6	4
Reactive stage	5	5
Duty (GJ/h)		
Condenser	66.14	107.63
Reboiler	62.93	104.42
Molar reaction conversion based on DCL2B feed flow rate	59.1%	59.1%

data of the liquid and vapor saturated enthalpies used in these Ponchon–Savarit diagrams are estimated from Aspen Plus, in which the reference state for enthalpy calculations is the component's constituent elements in an ideal gas state at 25°C and 1 atm, like all commercial simulators. Hence, the enthalpy difference points in Eqs. 33 and 34 are fixed as top and bottom difference points, since we do not have to include the heat of reaction in this elemental reference condition (Venkataraman et al., 1990). We also reflect the heat effect from the reaction on the slopes of the operating lines in a McCabe–Thiele diagram. We will present the simulation results from Aspen Plus and compare them with graphical results.

Deterimation of reaction zone by Ponchon–Savarit and McCabe–Thiele diagrams

We construct Ponchon–Savarit and McCabe–Thiele diagrams of the isomerization reaction (Eq. 42) by using stage-to-stage calculations from the top and bottom product compositions for given feed and product specifications with the same reaction conversion in Figures 11 and 12. The heat effect from the reaction does not significantly change the slopes of the operating lines in the McCabe–Thiele diagrams. The slopes are decreasing slightly for this exothermic reaction as we go up from the bottom product composition in Figure 11b and go down from the top in Figure 12b. The feed stream is a mixed vapor–liquid phase with molar compositions of 80% CYO and 20% ECP. The required purities of the top and bottom products are 95 mol % and 96 mol %.

It is better to locate the reaction zone in the stripping section than in the rectifying section, as the reactant, CYO, is lighter than the product, ECP. The total number of stages needed when the reaction takes place in the stripping section is seven stages including a reboiler (Figure 11). This is one stage less than the case where the reactive zone is located in the rectifying section (Figure 12). Furthermore, the heat demand is larger when the reaction takes place in the rectifying section, which can be explained through the positions of nonreactive difference points in the Ponchon–Savarit diagrams and the slopes of the operating lines in the McCabe–Thiele diagrams.

We perform computer simulations to verify the graphical results of the locations of reaction zones by using AspenPlus. The simulation results in Table 4 also clearly show an eco-

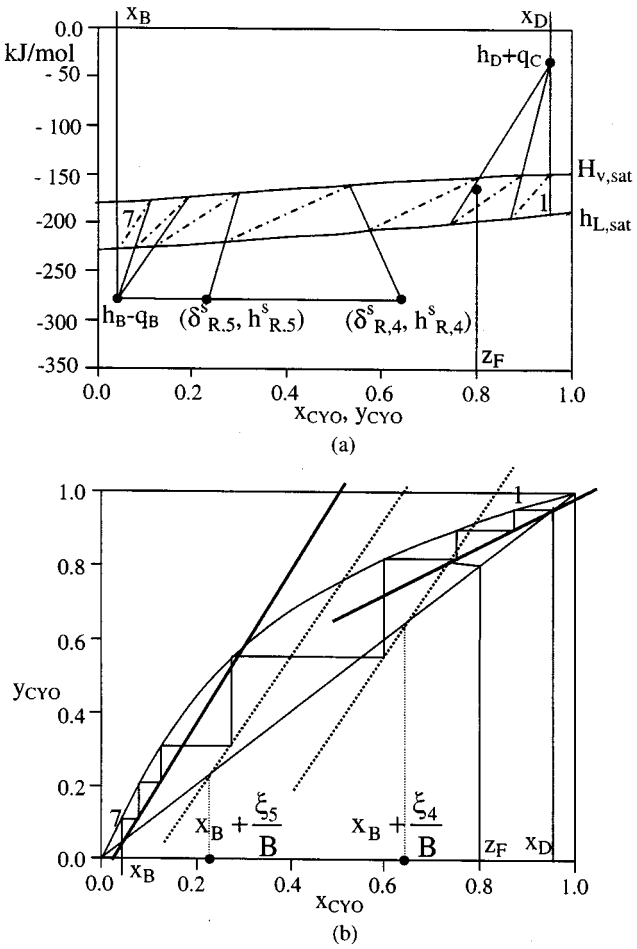

Figure 11. Graphical design for a reactive distillation column with the isomerization reaction of cyclohexanone oxime (CYO) to epsilon-caprolactam (ECP) in the stripping section.

(a) A Ponchon–Savarit diagram; (b) a McCabe–Thiele diagram.

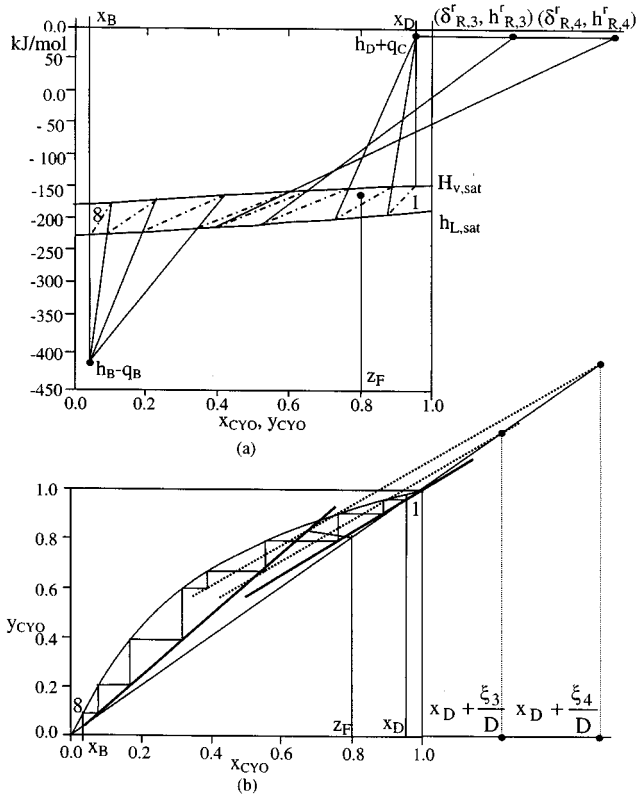

Figure 12. Graphical design for a reactive distillation column with the isomerization reaction of cyclohexanone oxime (CYO) to epsilon-caprolactam (ECP) in the rectifying section.

(a) A Ponchon–Savarit diagram; (b) a McCabe–Thiele diagram.

Table 4. Simulation Results for Both Reaction Zones in the Rectifying and Stripping Sections with the Isomerization in Eq. 42

Reaction Zones	Rectifying Section	Stripping Section
Feed stream		
Flow (kmol/h)	1000	1000
Mol fraction ECP/CYO	0.2/0.8	0.2/0.8
Product flow (kmol/h)		
Distillate flow CYO/purity	500/97.3%	500/97.3%
Bottom flow ECP/purity	500/99.0%	500/99.0%
Total number of stages	10	9
Feed stage	6	3
Reactive stages	4–5	4–5
Duty (GJ/h)		
Condenser	172.12	121.06
Reboiler	126.42	75.36
Molar reaction conversion based on CYO feed flow rate	38.5%	38.5%

nomic advantage for this isomerization reaction when the reaction zone is found in the stripping section. The overall number of stages is reduced from ten to nine and the duties in both the condenser and reboiler are reduced by around 30 and 40 %, respectively.

Reaction Distribution by Ponchon–Savarit Diagrams for Dimerization in a Column

Two identical components form one aggregated component in the dimerization reaction (Eq. 43). As this reaction changes the total number of moles in the reacting mixture, the heat of reaction is usually more dominant than binary isomerization reactions. Hence, we need to use the Ponchon–Savarit method rather than the McCabe–Thiele method to design a reactive distillation column with the dimerization or decomposition. Unlike the isomerization in the previous section, we employ the reaction difference point that is the ratio of the stoichiometric coefficient vector to the total sum of stoichiometric coefficients, $\delta_R = \boldsymbol{\nu}/\nu_T = [-2, 1]^T/(-1) = [2, -1]^T$. We can rewrite Eqs. 3 and 7, as Eqs. 44 and 45 for the reaction zones in the rectifying and stripping sections:

$$2\,R1 \Leftrightarrow P1 \tag{43}$$

$$V_{n+1} y_{n+1} - L_n x_n (D - \nu_T \xi_n)\,\delta^r_{R,\,n} \tag{44}$$

$$\overline{V}_{s+1} y_{s+1} - \overline{L}_s x_s = -(B - \nu_T \xi_{s+1})\,\delta^s_{R,\,s+1}, \tag{45}$$

where the reactive cascade difference points for the rectifying and stripping sections are as follows:

$$\delta^r_{R,\,n} = \frac{D x_D - \nu_T \xi_n \delta_R}{D - \nu_T \xi_n} \tag{46}$$

$$\delta^s_{R,\,s+1} = \frac{B x_B - \nu_T \xi_{s+1} \delta_R}{B - \nu_T \xi_{s+1}}. \tag{47}$$

We can obtain the heat balances for the reactive rectifying and stripping sections in Eqs. 48 and 49 by rearranging Eqs. 31 and 32:

$$V_{n+1} H_{n+1} - L_n h_n = (D - \nu_T \xi_n) h^r_{R,\,n} \tag{48}$$

$$\overline{V}_{s+1} H_{s+1} - \overline{L}_s h_s = -(B - \nu_T \xi_{s+1}) h^s_{R,\,s+1}, \tag{49}$$

where

$$h^r_{R,\,n} = \frac{D(h_D + q_C) - \nu_T \xi_n (-\Delta h_R/\nu_T)}{D - \nu_T \xi_n} \tag{50}$$

$$h^s_{R,\,s+1} = \frac{B(h_B - q_B) - \nu_T \xi_{s+1} (-\Delta h_R/\nu_T)}{B - \nu_T \xi_{s+1}}. \tag{51}$$

The slopes of the line connecting the reactive cascade difference points are also constant in a composition-enthalpy space for the given condenser and reboiler duties. The slopes for the rectifying and stripping sections are in Eqs. 52 and 53 if we consider the reaction difference point equal to 2 for component $R1$ whose derivation is available in Part B of the Appendix. In general, we understand that the enthalpy difference point $(h_D + q_C)$ at the distillate composition is greater than the heat of reaction $-\Delta h_R$ and the enthalpy difference point $(h_B - q_B)$ at the bottom composition is less than the heat of reaction $-\Delta h_R$, since the saturated vapor enthalpy is greater than the saturated liquid enthalpy for most of the binary mixtures in Eqs. 48 and 49, whose proof of this is available in Part C of the Appendix. If exothermic dimerization takes place in the rectifying section, the slope of the line connecting the reactive cascade difference points in Eq. 52 is always negative, as Δh_R is negative for an exothermic reaction, and $(h_D + q_C)$ should be larger than $-\Delta h_R$. In the same sense, the slope in Eq. 5 is always positive with the endothermic dimerization reaction in the stripping section, since Δh_R is positive and $(h_B - q_B)$ should be less than $-\Delta h_R$. The slope for the endothermic reaction in the rectifying section or the exothermic reaction in the stripping section can be negative or positive:

$$\frac{h^r_{R,\,n+1} - h^r_{R,\,n}}{\delta^r_{R,\,n+1,\,R1} - \delta^r_{R,\,n,\,R1}} = \frac{(h_D + q_C + \Delta h_R/\nu_T)}{(x_D - 2)} \tag{52}$$

$$\frac{h^s_{R,\,s} - h^s_{R,\,s+1}}{\delta^s_{R,\,s,\,R1} - \delta^s_{R,\,s+1,\,R1}} = \frac{(h_B - q_B + \Delta h_R/\nu_T)}{(x_B - 2)}. \tag{53}$$

We also assume that the saturated vapor and liquid enthalpies decrease as the mixture becomes more volatile due to the same behavior as most binary mixtures and that the heat of reaction is constant. Here, we consider the locations of the reaction zones in the rectifying and stripping sections for an exothermic reaction. The composition profile can be reversed with the rectifying reaction zone in Figure 13 even if we do not encounter a pinch point. Stages 3 and 4 show this fluctuation of compositions due to the reaction on reactive stages 2 and 3. The feed stage in this case is stage 4 and the number of stages required for the product specification is nine, including a reboiler. On the other hand, there is no reversal in the composition profile of Figure 14, and only five stages are needed with the reaction zone in the stripping sec-

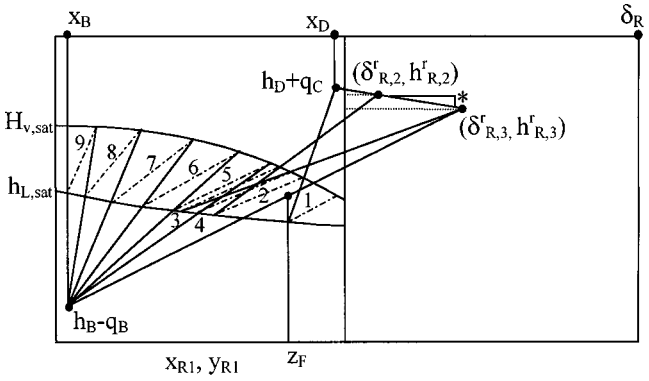

Figure 13. A Ponchon–Savarit diagram for reactive distillation with the dimerization reaction in the rectifying section.

∗: Constant slope in Eq. 52.

Table 5. Comparison of Simulation Results for both Reaction Zones in the Rectifying and Stripping Sections with the Dimerization Reaction in Eq. 54

Reaction Zones	Rectifying Section	Stripping Section
Feed stream		
Flow (kmol/h)	1000	1000
Mol fraction IBIB/IBA	0.1/0.9	0.1/0.9
Product flow (kmol/h)		
Distillate flow/IBA purity	200/99.2%	200/99.7%
Bottom flow/IBIB purity	449.87/99.7%	450.72/99.6%
Total number of stages	8	5
Reactive stages	4–5	3
Feed stage	6	2
Duty (GJ/h)		
Condenser	100.49	81.04
Reboiler	48.61	29.19
Molar reaction conversion based on IBA feed flow rate	77.8%	77.7%

tion for the same product specifications. As in the results of the locations of the reaction zones with the previous isomerization reaction, we should locate the reaction zone in the stripping section for a light reactant and a heavy product of the dimerization reaction. The symmetric results can conserve for a decomposition reaction with which we should construct the reaction zone in the rectifying section.

Here, we take the endothermic dimerization reaction of isobutyraldehyde (IBA), producing isobutylisobutyrate (IBIB) under aluminum isobutoxide catalyst in Eq. 54 as a case study for rigorous simulations. The reaction temperature is in the 90 to 140°C range (Hagemeyer and Wright, 1963). The boiling range of the mixture with IBA and IBIB at 1 atm is around 64 to 148°C, which overlaps with the reaction temperature. The relative volatility of IBA is 7.7 to 14.8 overall composition range. This reaction is endothermic and takes place in the liquid phase (Sittig, 1969):

$$2CH_3CHCH_3CHO\ (\text{IBA, light}) \Leftrightarrow CH_3CHCH_3COOCH_2CHCH_3CH_3(\text{IBIB, heavy}). \quad (54)$$

Table 5 shows the simulation results for two cases of the reactive rectifying and stripping sections. In terms of the number of stages, and duties of a condenser and a reboiler, the case of the stripping reaction zone is better than that of the rectifying reaction zone.

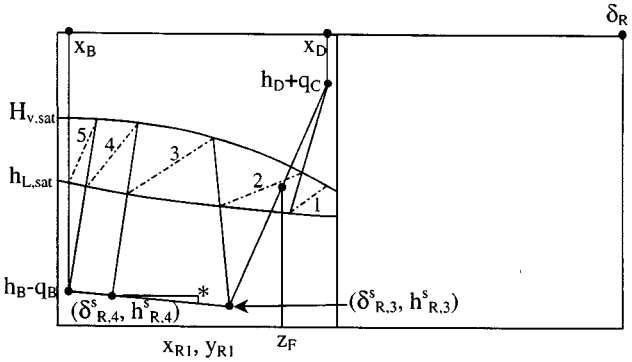

Figure 14. A Ponchon–Savarit diagram for reactive distillation with the dimerization reaction in the stripping section.

∗: Constant slope in Eq. 53.

Reaction Distribution for the Feed Composition Outside the Product Compositions

Due to the reaction in reactive distillation, the feed composition can be outside the product compositions in the McCabe–Thiele and Ponchon–Savarit diagrams, especially when the feed stream contains a pure reactant. We deal with the same reaction (Eq. 1) taking place in the rectifying section and treat the case in which the bottom product is less pure than the feed stream in a McCabe–Thiele diagram. If the bottom composition lies to the right of the feed composition, the material balance around the reactive distillation column in Eqs. 10 and 11 mandates that the final difference point should be to the left of the feed composition in Figure 15.

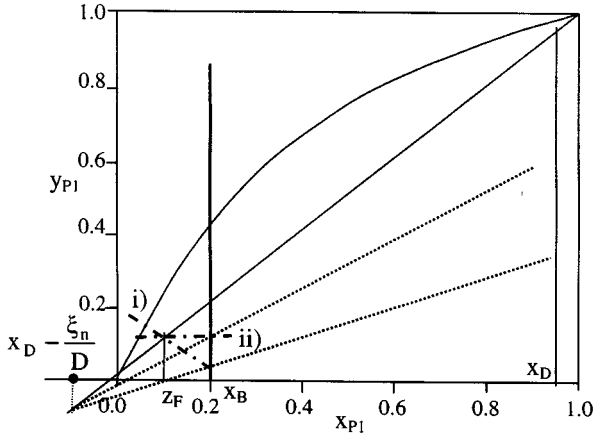

Figure 15. The construction of the *q*-line when the final difference point of the top transcends the feed composition and the slope of the bottom operating line is infinite.

(i) The *q*-line for the feed stream with mixed phases; (ii) the *q*-line for the saturated vapor feed stream.

In this case, the operating lines move further down than the operating lines in Figure 2, which reduces the number of stages required for product specifications. The bottom operating line and the final rectifying operating line will meet below the 45 degree line. Hence, there is no pinch point from the minimum reflux in nonreactive distillation. The bottom operating line can be a vertical line parallel to the ordinate, which means zero boiling in the reboiler. Thus, the slope of the operating line can be infinite for all thermal conditions of the feed stream except the saturated and subcooled liquid feeds in Figure 15. If the bottom operating line is infinite, the slopes of the final rectifying operating lines (dotted lines in Figure 15) will decrease as the thermal condition of the feed stream switches from the saturated vapor to the mixed phase in Figure 15.

Intuitively, this suggests that when the bottom product is less pure than the feed stream, we can design a reactive distillation column without a reboiler. Even if the feed stream is a saturated or subcooled liquid, the stripping operating line and the final rectifying operating line do not meet between the equilibrium curve and the 45-degree line. Hence, the minimum reflux pinch cannot occur. However, we need a heating source in the reboiler for the feed stream with saturated and subcooled liquids.

On the other hand, if we locate the reaction zone in the stripping section for the case in which the feed composition lies outside the product compositions, a pinch point occurs for a certain reaction conversion in the same way as in Figure 3.

Conclusions

We show the design implications of locating the reaction zones in a reactive distillation column for binary isomerization and dimerization reactions by using the McCabe–Thiele and Ponchon–Savarit methods. If the reaction has a heavy reactant and a light product, the reaction zone should be in the rectifying section to enhance the separation efficiency and to avoid possible pinch points. Conversely, with a light reactant and a heavy product in the reaction, we should construct the reaction zone in the stripping section. These results still hold for a reactive system with a prominent heat of reaction. While the McCabe–Thiele diagrams are easy and accurate for designing a reactive distillation column with an isomerization reaction, the Ponchon–Savarit method is suitable for isomerization reactions with dominant heat effects as well as dimerization reactions causing the change in the overall number of moles. These graphical methods can contribute to design improvements from the visualization of the reactive distillation process, for instance, how reactive distillation circumvents a binary azeotrope (Lee et al., 2000d). At present these methods are limited to binary mixtures. However, the analysis of the binary systems has revealed a number of basic steps that are important while extending the methods and insights to ternary and quaternary component systems.

Notation

B = bottom molar flow rate
c_P = the normalized product coefficient vector
c_P = the normalized product coefficient (scalar)
c_R = the normalized reactant coefficient (scalar)
D = distillate molar flow rate
F = feed molar flow rate
$\hat{F}$ = pseudofeed molar flow rate
h_B = molar enthalpy in the bottom product
h_D = distillate molar enthalpy
h_F = feed molar enthalpy
h_i = liquid molar enthalpy at stage i
H_i = vapor molar enthalpy at stage i
h_L = constant liquid molar enthalpy in a column
H_V = constant vapor molar enthalpy in a column
L = liquid molar flow rate going down from the feed stage
$\overline{L}$ = liquid molar flow rate going up to the feed stage
L_n = liquid molar flow rate at stage n in the rectifying section
$\overline{L}_s$ = liquid molar flow rate at stage s in the stripping section
Pk = product of component k
q = liquid fraction of the feed
Q_B = duty of a reboiler
q_C = molar duty of a condenser
Δh_R = heat of reaction
Ri = reactant of component i
V_n = vapor molar flow rate at stage n in the rectifying section
V = vapor molar flow rate going up from the feed stage
$\overline{V}$ = vapor molar flow rate going up to the feed stage
$\overline{V}_s$ = vapor molar flow rate at stage s in the stripping section
x_B = liquid composition vector for the bottom product
x_B = liquid composition for the bottom product (scalar)
x_D = liquid composition vector for the distillate product
x_n = liquid composition vector at stage n
x_n = liquid composition at stage n (scalar)
y_n = vapor composition vector at stage n
y_n = vapor composition at stage n (scalar)
z_F = feed composition vector
z_F = feed composition (scalar)
$z_{\hat{F}}$ = pseudofeed composition vector
ξ = total molar reaction turnover flow rate

Literature Cited

Agreda, V. H., and L. R. Partin, "Reactive Distillation Process for the Production of Methyl Acetate," U.S. Patent No. 4,435,595 (1984).

Agreda, V. H., L. R. Partin, and W. H. Heise, "High Purity Methyl Acetate via Reactive Distillation," *Chem. Eng. Prog.*, **86**(2), 40 (1990).

Balashov, M. I., and L. A. Serafimov, "Analysis of Statics of Continuous Combined Reaction-Fractionation Process," *Theor. Found. Chem. Technol.*, **14**, 495 (1980).

Barbosa, D., and M. F. Doherty, "Theory of Phase Diagrams and Azeotropic Conditions for Two-Phase Reactive System," *Proc. R. Soc. London*, **A413**, 443 (1987a).

Barbosa, D., and M. F. Doherty, "A New Set of Composition Variables for the Representation of Reactive Phase Diagram," *Proc. R. Soc. London*, **A413**, 459 (1987b).

Barbosa, D., and M. F. Doherty, "Design and Minimum-Reflux Calculations for Single-Feed Multicomponent Reactive Distillation Columns," *Chem. Eng. Sci.*, **43**, 1523 (1988a).

Barbosa, D., and M. F. Doherty, "Design and Minimum-Reflux Calculations for Double-Feed Multicomponent Reactive Distillation Columns," *Chem. Eng. Sci.*, **43**, 2377 (1988b).

Bell, W. K., and W. O. Haag, "Synthesis of Caprolactam," U.S. Patent No. 4,927,924 (1990).

Bell, W. K., and C. D. Chang, "Process for Making Epsilon-Caprolactam," U.S. Patent No. 4,359,421 (1982).

Bessling, B., G. Schembecker, and K. H. Shimmrock, "Design of Processes with Reactive Distillation Line Diagrams," *Ind. Eng. Chem. Res.*, **36**, 3032 (1997).

Buzad, G., and M. F. Doherty, "Design of Three-Component Kinetically Controlled Reactive Distillation Columns Using Fixed-Point Methods," *Chem. Eng. Sci.*, **49**, 1947 (1994).

Buzad, G., and M. F. Doherty, "New Tools for Design of Kinetically Controlled Reactive Distillation Columns for Ternary Mixtures," *Comput. Chem. Eng.*, **19**, 395 (1995).

Costain, W., and B. W. H. Terry, "Allylic Rearrangement of Dichlorobutenes," U.S. Patent No. 3,342,882 (1967).
Daubert, T. E., R. P. Danner, H. M. Sibul, and C. C. Stebbins, *Physical and Thermodynamic Properties of Pure Chemicals: Data Compilation*, Hemisphere, New York (1989).
DeGarmo, J. L., V. N. Parulekar, and V. Pinjala, "Consider Reactive Distillation," *Chem. Eng. Prog.*, **88**(3), 43 (1992).
Doherty, M. F., "A Topological Theory of Phase Diagrams for Multiphase Reacting Mixtures," *Proc. R. Soc. London*, **A430**, 669 (1990).
Espinosa, J., N. Scenna, and G. Perez, "Graphical Procedure for Reactive Distillation Systems," *Chem. Eng. Commun.*, **119**, 109 (1993).
Gehrmann, K., A. Ohorodnik, O. Dettmeier, and H. Berns, "Process for the Continuous Manufacture of 3,4-dichlorobutene-1," U.S. Patent No. 3,890,399 (1975).
Giessler, S., R. Y. Danilov, Y. A Pisarenko, L. A. Serafimov, S. Hasebe, and I. Hashimoto, "Feasibility Study of Reactive Distillation Using the Analysis of the Statics," *Ind. Eng. Chem. Res.*, **37**, 4375 (1998).
Hagemeyer, H. J., and H. N. Wright, "Preparation of Esters by Aldehyde Condensation," U.S. Patent No. 3,081,344 (1963).
Harris, A. T., and D. A. Melchert, "Dichlorobutene Isomerization Process," U.S. Patent No. 4,827,059 (1989).
Hauan, S., PhD Thesis, Norwegian Univ. of Science and Technology, Trondheim, Norway (1998).
Hauan, S., T. Omtveit, and K. M. Lien, "Analysis of Reactive Separation Systems," AIChE Meeting, Chicago, IL (1996).
Hauan, S., A. W. Westerberg, and K. M. Lien, "Phenomena Based Analysis of Fixed Points in Reactive Separation Systems," *Chem. Eng. Sci.*, **55**, 1053 (1999).
Hauan, S., A. R. Ciric, A. W. Westerberg, and K. M. Lien, "Difference Points in Extractive and Reactive Cascades. I—Basic Properties and Analysis," *Chem. Eng. Sci.*, **55**, 3145 (2000).
Hearne, G. W., and D. S. LaFrance, "Rearrangement Process," U.S. Patent No. 2,446,475 (1948).
Ho, F. G., and G. E. Keller, "Process Integration," *Recent Developments in Chemical Process and Plant Design*, Y. A. Liu, H. A. McGee, and W. R. Epperly, eds., Wiley, New York (1987).
Kadowaki, T., T. Iwasaki, and H. Matsumura, "Method of Isomerizing Dichlorobutenes," U.S. Patent No. 3,927,130 (1975).
Kajikuri, H., M. Kitamura, and Y. Higashio, "Process for Producing Epsilon-Caprolactam," U.S. Patent No. 5,304,643 (1994).
Kitamura, M., H. Ichihashi, G. Suzukamo, and Y. Nakamura, "Process for Producing .Epsilon.-caprolactam," U.S. Patent No. 4,968,793 (1990).
Lee, J. W., S. Hauan, K. M. Lien, and A. W. Westerberg, "Difference Points in Extractive and Reactive Cascade II—Generating Design Alternatives by Lever Rule for Reactive Systems," *Chem. Eng. Sci.*, **55**, 3161 (2000a).
Lee, J. W., S. Hauan, K. M. Lien, and A. W. Westerberg, "A Graphical Method for Designing Reactive Distillation Columns I—The Ponchon-Savarit Diagram," *Proc. R. Soc. London*, in press (2000b).
Lee, J. W., S. Hauan, K. M. Lien, and A. W. Westerberg, "A Graphical Method for Designing Reactive Distillation Columns II—The McCabe-Thiele Diagram," *Proc. R. Soc. London*, in press (2000c).
Lee, J. W., S. Hauan, and A. W. Westerberg, "Circumventing an Azeotrope in Reactive Distillation," *Ind. Eng. Chem. Res.*, **39**, 1061 (2000d).
Okasinski, M. J., and M. F. Doherty, "Design Method for Kinematically Controlled, Staged Reactive Distillation Columns," *Ind. Eng. Chem. Res.*, **37**, 2821 (1998).
Pisarenko, Y. A., and L. A. Serafimov, "A Steady States for a Reactive-Distillation Process Column with One Product Stream," *Theor. Found. Chem. Technol.*, **21**, 281 (1988).
Pisarenko, Y. A., R. Y. Danilov, and L. A. Serafimov, "Infinite-Efficiency Operating Conditions in Analysis of the Statics of Reactive Rectification," *Theor. Found. Chem. Technol.*, **29**, 556 (1995).
Pisarenko, Y. A., R. Y. Danilov, and L. A. Serafimov, "Application of the Concept of Limiting Paths to Estimating the Feasibility of Steady States in Analyzing the Statics of Reactive Rectification Processes," *Theor. Found. Chem. Technol.*, **31**, 43 (1997).
Sato, H., K. Hirose, M. Kitamura, H. Tojima, and N. Ishii, "Process for Producing Epsilon-Caprolactam," U.S. Patent No. 4,717,770 (1988).
Sato, H., K. Hirose, N. Ishii, and Y. Umada, "Process for Producing Epsilon-Caprolactam," U.S. Patent No. 4,709,024 (1987).
Siirola, J. J., "An Industrial Perspective on Process Synthesis," *AIChE Symp. Ser.*, **304**, 222 (1995).
Sittig, M., *Organic Chemical Process Encyclopedia*, 2nd ed., Noyes Development Corp., Park Ridge, NJ (1969).
Stichlmair, J. G., and J. R. Fair, *Distillation: Principle and Practice*, Wiley-VCH, New York (1998).
Terranova, B. E., and A. W. Westerberg, "Temperature-Heat Diagrams for Complex Columns. I. Intercooled/Interheated Distillation Columns," *Ind. Eng. Chem. Res.*, **28**, 1374 (1989).
Venkataraman, S., W. K. Chan, and J. F. Boston, "Reactive Distillation Using Aspen Plus," *Chem. Eng. Prog.*, **86**(8), 45 (1990).
Yashima, T., and T. Komatsu, "Process for Producing Epsilon-Caprolactam," U.S. Patent No. 5,312,915 (1994).

Appendix

A. Derivation of Eq. 22

In general, the reactive operating lines are as follows for the $(n-1)$ stage and the n stage from the top:

$$y_n = \frac{L_{n-1}}{V_n} x_{n-1} + \frac{D}{V_n} x_D - \frac{\xi_{n-1}}{V_n} \tag{A1}$$

$$y_{n+1} = \frac{L_n}{V_{n+1}} x_n + \frac{D}{V_{n+1}} x_D - \frac{\xi_n}{V_{n+1}}. \tag{A2}$$

In terms of total balance around the rectifying section of the isomerization reaction ($\nu_T = 0$) in Eq. 2, we have the following equations (Eqs. A3 and A4) for the nth stage:

$$V_{n+1} = L_n + D \tag{A3}$$

$$1 = \frac{L_n}{V_{n+1}} + \frac{D}{V_{n+1}}. \tag{A4}$$

If we have an exothermic reaction in the rectifying section, the liquid flow rate will decrease as we go down the column and this will also reduce the vapor flow rate in Eq. A3. Hence, D/V_{n+1} will increase and the slope L_n/V_{n+1} will decrease. If the slopes of the operating lines are decreasing, the y-intercepts can increase or decrease. But to have a better separation performance from a larger gap between the equilibrium curve and the operating line in Figure 5b, the $y-$intercepts should be decreasing as we go down the column in Eq. A5. We can arrange Eq. A5 into A6:

$$\frac{D}{V_{n+1}} x_D - \frac{\xi_n}{V_{n+1}} < \frac{D}{V_n} x_D - \frac{\xi_{n-1}}{V_n} \tag{A5}$$

$$\frac{(Dx_D - \xi_{n-1})V_{n+1} - (Dx_D - \xi_n)V_n}{V_n V_{n+1}} > 0. \tag{A6}$$

In Eq. A6, the denominator is always positive and the numerator should be greater than zero. By letting V_n be $(V_n + V_{n+1} - V_{n+1})$ in the numerator of Eq. A6, we rearrange the numerator and obtain Eq. A7. Since V_{n+1} is always greater than $(Dx_D - \xi_n)$, the denominator of the left term in Eq. A7, $(V_n$

$-V_{n+1}$), should be equal to or less than the denominator of the right term in Eq. A7, $(\xi_n - \xi_{n-1})$, like Eq. A8, which is identical to Eq. 22:

$$\frac{V_{n+1}}{V_n - V_{n+1}} > \frac{Dx_D - \xi_n}{\xi_n - \xi_{n-1}} \tag{A7}$$

$$(V_n - V_{n+1}) \le (\xi_n - \xi_{n-1}). \tag{A8}$$

B. Proof of the constant slopes for reactive cascade difference points in Ponchon–Savarit diagrams

1. Derivation of Eq. 37: From Eqs. 33 and 26, we can write the following equation and easily get the slope $-\Delta h_R$ by simple manipulations:

$$\frac{h^r_{R,\,n+1} - h^r_{R,\,n}}{\delta^r_{R,\,n+1,\,P1} - \delta^r_{R,\,n,\,P1}} = \frac{(h_D + q_C + \Delta h_R \xi_{n+1}/D) - (h_D + q_C + \Delta h_R \xi_n/D)}{(x_D - \xi_{n+1}/D) - (x_D - \xi_n/D)} = -\Delta h_R. \tag{A9}$$

2. Derivation of Eq. 38: From Eqs. 33 and 27, we obtain the following equation and easily get the slope Δh_R by simple manipulations:

$$\frac{h^r_{R,\,n+1} - h^r_{R,\,n}}{\delta^r_{R,\,n+1,\,R1} - \delta^r_{R,\,n,\,R1}} = \frac{(h_D + q_C + \Delta h_R \xi_{n+1}/D) - (h_D + q_C + \Delta h_R \xi_n/D)}{(x_D + \xi_{n+1}/D) - (x_D + \xi_n/D)} = \Delta h_R. \tag{A10}$$

3. Derivation of Eq. 39: If we substitute Eqs. 34 and 29 into Eq. 39, we obtain Eq. A11 easily by rearrangement:

$$\frac{h^s_{R,\,s} - h^s_{R,\,s+1}}{\delta^s_{R,\,s,\,P1} - \delta^s_{R,\,s+1,\,P1}} = \frac{(h_B - q_B + \Delta h_R \xi_s/B) - (h_B - q_B + \Delta h_R \xi_{s+1}/B)}{(x_B - \xi_s/B) - (x_B - \xi_{s+1}/B)} = -\Delta h_R. \tag{A11}$$

4. Derivation of Eq. 40: As before, we obtain Eq. A12 by substituting Eqs. 34 and 30 into Eq. 40:

$$\frac{h^s_{R,\,s} - h^s_{R,\,s+1}}{\delta^s_{R,\,s,\,R1} - \delta^s_{R,\,s+1,\,R1}} = \frac{(h_B - q_B + \Delta h_R \xi_s/B) - (h_B - q_B + \Delta h_R \xi_{s+1}/B)}{(x_B + \xi_s/B) - (x_B + \xi_{s+1}/B)} = \Delta h_R. \tag{A12}$$

5. Derivation of Eq. 52: Substituting Eqs. 46 and 50 into Eq. 52 by considering the indices of the stage number and letting the reaction difference point, δ_R, be equal to 2 for component $R1$, we obtain Eq. A13:

$$\frac{h^r_{R,\,n+1} - h^r_{R,\,n}}{\delta^r_{R,\,n+1,\,P1} - \delta^r_{R,\,n,\,P1}} = \frac{\left(\dfrac{D(h_D + q_C) - \nu_T \xi_{n+1}(-\Delta h_R/\nu_T)}{D - \nu_T \xi_{n+1}} - \dfrac{D(h_D + q_C) - \nu_T \xi_n(-\Delta h_R/\nu_T)}{D - \nu_T \xi_n}\right)}{\left(\dfrac{Dx_D - \nu_T \xi_{n+1}\delta_R}{D - \nu_T \xi_{n+1}} - \dfrac{Dx_D - \nu_T \xi_n \delta_R}{D - \nu_T \xi_n}\right)} = \frac{(h_D + q_C + \Delta h_R/\nu_T)}{(x_D - 2)}. \tag{A13}$$

6. Derivation of Eq. 53: Substituting Eqs. 47 and 51 into Eq. 53 by considering the indices of the stage number and letting the reaction difference point, δ_R, equal to 2 for component $R1$, we obtain Eq. A14:

$$\frac{h^s_{R,\,s} - h^s_{R,\,s+1}}{\delta^s_{R,\,s,\,R1} - \delta^s_{R,s+1,\,R1}} = \frac{\left(\dfrac{B(h_B - q_B) - \nu_T \xi_{s+1}(-\Delta h_R/\nu_T)}{B - \nu_T \xi_{s+1}} - \dfrac{B(h_B - q_B) - \nu_T \xi_s(-\Delta h_R/\nu_T)}{D - \nu_T \xi_s}\right)}{\left(\dfrac{Bx_B - \nu_T \xi_{s+1}\delta_R}{B - \nu_T \xi_{s+1}} - \dfrac{Bx_B - \nu_T \xi_s \delta_R}{B - \nu_T \xi_s}\right)} = \frac{(h_B - q_B + \Delta h_R/\nu_T)}{(x_B - 2)}. \tag{A14}$$

C. Proofs that the top enthalpy difference point is greater than the heat of reaction and the bottom difference point is less than the heat of reaction

The heat balances around the rectifying and stripping reaction zones are in (Eqs. A15) and A16:

$$V_{n+1}H_{n+1} - L_n h_n = D(h_D + q_C) + \Delta h_R \xi_n \quad \text{(A15)}$$

$$\overline{V}_{s+1}H_{s+1} - \overline{L}_s h_s = -B(h_B - q_B) - \Delta h_R \xi_{s+1}. \quad \text{(A16)}$$

As the terms on the left side of Eqs. A15 and A16 are greater than zero, we have the following relationships. For any reaction molar turnover flow rates, $(h_D + q_C)$ is larger than $-\Delta h_R$ and $(h_B - q_B)$ is less than $-\Delta h_R$:

$$(h_D + q_C) > \frac{\xi_n}{D}(-\Delta h_R) \quad \text{(A17)}$$

$$(h_B - q_B) < \frac{\xi_{s+1}}{B}(-\Delta h_R). \quad \text{(A18)}$$

Manuscript received May 3, 1999, and revision received Dec. 28, 1999.